Effects of cobalt additive on amorphous vanadium phosphate catalysts prepared using precipitation with supercritical CO_2 as an antisolvent

J. Antonio Lopez-Sanchez,[a] Jonathan K. Bartley,[a] Andrew Burrows,[b] Christopher J. Kiely,†[b] Michael Hävecker,[c] Robert Schlögl,[c] Jean Claude Volta,[d] Martin Poliakoff[e] and Graham J. Hutchings*[a]

[a] *Department of Chemistry, Cardiff University, P O Box 912, Cardiff, UK CF10 3TB. E-mail: hutch@cf.ac.uk*
[b] *Departments of Engineering and Chemistry, University of Liverpool, Liverpool, UK L69 3BX*
[c] *Department of Inorganic Chemistry, Fritz-Haber – Institute der Max-Planck-Gesellschaft, Faradayweg 4–6, D-14195, Berlin, Germany*
[d] *Institut de Recherches sur la Catalyse, CNRS, 2 Avenue Albert Einstein, 69626, Villeurbanne cedex, France*
[e] *School of Chemistry, University of Nottingham, University Park, Nottingham, UK NG7 2RD*

Received (in Montpellier, France) 10th June 2002, Accepted 4th September 2002
First published as an Advance Article on the web 29th October 2002

The effect of addition of cobalt to an amorphous vanadium phosphate for the selective oxidation of *n*-butane to maleic anhydride is described and discussed. Cobalt is a well known promoter for crystalline vanadium phosphate catalysts and is most effective at a concentration of 1 atom % relative to vanadium. In contrast, for amorphous vanadium phosphate materials, prepared by precipitation using supercritical CO_2 as an antisolvent, cobalt appears to act as a catalyst poison, decreasing both the catalyst activity and selectivity for maleic anhydride. Detailed analysis by transmission electron microscopy, ^{31}P spin echo mapping NMR spectroscopy and X-ray absorption spectroscopy is described, which highlight differences with the unmodified catalyst. It is concluded that the addition of cobalt affects the morphology of the material and the oxidation state of vanadium, and that these changes deleteriously affect the catalytic performance.

Promotion of heterogeneous catalysts is a topic that is of immense industrial and academic importance.[1–4] The topic has been well studied for vanadium phosphate catalysts for the selective oxidation of *n*-butane to maleic anhydride.[5,6] For many years, the study of vanadium phosphate catalysts has focussed on a range of crystalline materials. In particular, the crystalline precursor $VOHPO_4{\cdot}0.5H_2O$ has received the greatest attention. This material is transformed *in situ* in *n*-butane/air at 400 °C to form a range of crystalline compounds, such as $(VO)_2P_2O_7$, α_{II}-$VOPO_4$ or δ-$VOPO_4$. These transformations are topotactic in nature and the epitaxial relationships have been determined using high resolution electron microscopy.[7] A number of additives in low concentration (typically 1 atom % relative to the vanadium concentration) are known to promote the catalytic performance of these vanadium phosphates. For example, Co and Fe both increase the catalytic activity, whereas Mo enhances the selectivity to maleic anhydride by decreasing the over-oxidation to carbon oxides.[6] Recently, we have followed the transformation of a Co-promoted catalyst using high resolution electron microscopy and ^{31}P NMR spectroscopy. Interestingly, we observed that Co was not readily soluble in crystalline $(VO)_2P_2O_7$, but was instead concentrated in the residual amorphous material in the catalyst.[8] This indicated that Co may be exerting its promotional affect in the amorphous vanadium phosphate, rather than $(VO)_2P_2O_7$ or other crystalline phases. This is in contrast to Fe as a promoter, since solid solutions having the general formula $[(VO)_xFe_{1-x}]_2P_2O_7$ have been reported to be significantly more active than pure $(VO)_2P_2O_7$.[9]

The subject of amorphous vanadium phosphates and their contribution to the catalytic performance has received considerable interest.[7,10–29] Indeed, it is considered by many researchers that highly crystalline $(VO)_2P_2O_7$ platelets have amorphous surface layers, and the active sites for *n*-butane oxidation may therefore be present within this amorphous material.[30] Recently, we have prepared a vanadium phosphate catalyst using a precipitation method that uses supercritical CO_2 as an antisolvent. The material is wholly amorphous and remains amorphous during reaction with *n*-butane and, furthermore, gives a higher intrinsic activity (mol maleic anhydride m^{-2} h^{-1}) than corresponding crystalline materials.[30] In view of this development we have examined the incorporation of Co (1 at %) into this new preparation method and in this paper we describe its effect on the catalytic performance and the structure of the material.

Experimental

Catalyst preparation

Preparation of crystalline $VOHPO_4{\cdot}0.5H_2O$. The hemihydrate $VOHPO_4{\cdot}0.5H_2O$ was prepared using the VPO route. The *VPO hemihydrate* was prepared by refluxing V_2O_5 (11.8 g, Strem) with H_3PO_4 (16.49 g, 85%, Aldrich) in isobutanol (250 ml) for 16 h. The light blue solid was recovered by filtration, washed with isobutanol (200 ml) and ethanol (150 ml, 100%). The solid was refluxed in water (9 ml H_2O per g solid)

† Present address: Department of Science and Engineering, Lehigh University, 5 East Packer Avenue, Bethlehem, PA 18015-3195, USA.

for 1 h, filtered hot, and dried in air (110 °C, 16 h). A cobalt promoted sample (1 atom % Co/V) was prepared using the same procedure, except that cobalt acetylacetonate (0.153 g) was added with the V_2O_5 and H_3PO_4 in the initial step of the preparation.

Catalyst preparation using supercritical CO_2 as an antisolvent. A solution of H_3PO_4 (1.8 g, 100%, Aldrich) in isopropanol (120 ml) was refluxed with $VOCl_3$ (1.6 ml, Aldrich) for 16 h to give a blue solution. The resulting isopropanol solution was processed using supercritical CO_2 to precipitate a vanadium phosphate. The isopropanol solution was pumped through a fine capillary (220 μm i.d.) into a precipitation vessel containing concurrently flowing CO_2. The CO_2 can act as an effective antisolvent when it is either a liquid (>42 bar at 20 °C) or a supercritical fluid ($T_c = 31.3$ °C, $P_c = 72$ bar). CO_2 was pumped as a liquid using a modified HPLC pump at pressures up to 110 bar; the system pressure is maintained by a back pressure regulator and flow rates of the CO_2 and isopropanol solution can be set independently. To achieve supercritical conditions, the precipitation vessel is held in a GC oven, allowing control of the temperature from ambient to *ca.* 100 °C. The CO_2 passes through a length of coiled tubing in the oven and is heated through its critical point, becoming supercritical. As the vanadium phosphate solution exits the capillary, the alcohol and CO_2 diffuse into each other, causing the isopropanol to expand, hence reducing its solvent power. The higher temperature, together with the removal of the organic solvent, enable rapid precipitation of the vanadium phosphate. This catalyst precursor (denoted VPO_{SCP}) was collected on a filter bed. The isopropanol solution was pumped at 0.1 ml min^{-1} through the capillary around which excess CO_2 was pumped at 7 ml min^{-1}. The system pressure was held constant at 110 bar and the precipitation vessel maintained at 60 °C. Experiments were typically conducted for 3 h, which resulted in the synthesis of approximately 0.2 g of solid.

Two further catalyst precursors were prepared using similar methodologies. First a Co-containing material was prepared using supercritical CO_2 precipitation for a modified solution containing 1 atom % Co. Cobalt acetylacetonate (0.0288 g, Aldrich) was dissolved in the isopropanol vanadium phosphate solution previously described (100 ml) and the resulting solution was refluxed for 5 h. This solution was then processed using supercritical CO_2 as described previously. Secondly, a solution was prepared by adding just acetylacetone (0.084 g, Aldrich) to the isopropanol vanadium phosphate solution (250 ml) and the resulting solution was refluxed for 5 h, prior to being processed using supercritical CO_2 as described above.

Catalyst testing

The oxidation of *n*-butane was carried out using a microreactor with a standard mass of catalyst (0.5 g). *n*-Butane and air were fed to the reactor *via* calibrated mass flow controllers to give a feedstock composition of 1.5% *n*-butane in air. The products were then fed *via* heated lines to an on-line gas chromatograph for product analysis. The reactor comprised a stainless steel tube with the catalyst held in place by plugs of quartz wool. A thermocouple was located in the centre of the catalyst bed and the temperature control was effective to ±1 °C. Carbon mass balances of ⩾97% were typically observed. Catalyst precursors were heated *in situ* (1.5% *n*-butane in air) by ramping the sample from room temperature to 400 °C at a rate of 3 °C min^{-1}.

Catalyst characterisation

A number of complimentary techniques were used to characterise the catalyst structure. Powder X-ray diffraction (XRD) was performed using an Enraf Nonius FRS90 X-ray generator with a Cu–K_α source and fitted with an Inel CPS 120 hemispherical detector. BET surface area measurements using nitrogen adsorption were carried out using a Micromeritics ASAP 2000 instrument. Electron microscopy observations were made with a JEOL 2000 EX high-resolution electron microscope (HREM) operating at 200 kV. The instrument had been fitted with a low-light-level TV camera and frame-averaging system to allow us to use very low illumination conditions. This latter condition is essential for studying these beam-sensitive vanadium phosphorous oxide compounds. Samples suitable for TEM analysis were prepared by dispersing the catalyst powder onto a lacey carbon film supported on a copper mesh grid.

The ^{31}P NMR measurements were performed on a Bruker MSL 300 NMR spectrometer. The ^{31}P spin echo mapping method has been shown by Li *et al.*[31] and Sananes *et al.*[32] to be a very powerful technique for evaluating the relative proportion of V^{5+} and V^{4+} ions surrounding the P atoms in vanadium phosphate compounds, independently of the crystallinity. The ^{31}P NMR spin echo spectra were recorded under static conditions, using a $90°x$-τ–$180°y$-τ acquisition sequence. The 90° probe duration was 4.2 μs and τ was 20 μs. For each sample, the irradiation frequency was varied in increments of 100 kHz above and below the ^{31}P resonance of H_3PO_4. The number of spectra recorded was dictated by the frequency limits beyond which no spectral intensity was detectable. The ^{31}P NMR spin echo mapping information was then obtained by superposition of all the spectra.

The X-ray absorption spectroscopy (XAS) experiments were performed with a special reactor cell consisting of two stainless-steel chambers. Details concerning the experimental set-up and the data processing can be found in the literature.[33–35] Experiments were carried out at the undulator beamline UE/56-2 at the third generation Berliner Synchrotron Radiation Facility BESSY II.[36] The near edge X-ray absorption fine structure (NEXAFS), that is, the strong variations of the absorption coefficient just at the absorption edge, were analysed in some detail. The photon energy of the NEXAFS spectra was calibrated by the π* resonance of molecular oxygen at 530.8 eV. The resolving power $E/\Delta E$ was about 3000. Vanadium L_3-edge spectra were analysed by least squares fitting using Gauss–Lorentz profiles to take into account experimental and intrinsic broadening.

Results and discussion

Catalyst evaluation

Five catalysts were evaluated for *n*-butane oxidation. These were: (*a*) VPO, a standard crystalline unpromoted $VOHPO_4{\cdot}0.5H_2O$ prepared using the VPO method; (*b*) VPO_{Co}, $VOHPO_4{\cdot}0.5H_2O$ containing 1 atom % Co; this material has been previously characterised;[8] (*c*) VPO_{SC}, precipitation using supercritical CO_2 in the absence of Co and acetylacetone; (*d*) VPO_{SCCo}, precipitation using supercritical CO_2 with 1% cobalt acetylacetonate; and (*e*) VPO_{SCacac}, precipitation using supercritical CO_2 with 1% acetylacetone. These precursors were evaluated as catalysts for the conversion of *n*-butane to maleic anhydride and the results for VPO_{SC}, VPO_{SCCo} and VPO_{SCacac} are shown in Fig. 1. In addition, the comparison of the intrinsic activity of all five catalysts is shown in Table 1. In addition, the effect of time-on-line during the initial reaction period is shown for representative catalysts in Fig. 2. The surface areas for the three materials prepared using precipitation with supercritical CO_2 are very similar at 4, 5 and 9 $m^2\ g^{-1}$ for VPO_{SC}, VPO_{SCCo} and VPO_{SCacac}, respectively. Cobalt acetylacetate was used as a source of Co in these studies as it was the source we previously used in our detailed study of the morphology of crystalline VPO catalysts.[8]

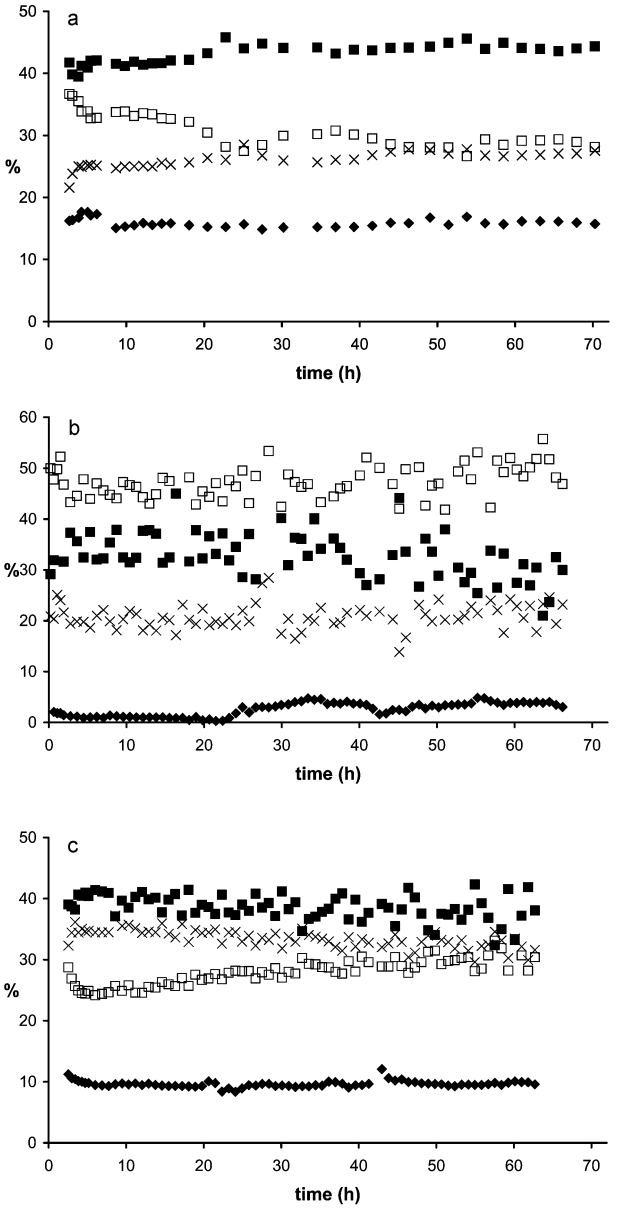

Fig. 1 Catalytic performance of vanadium phosphates for the oxidation of *n*-butane. Reaction conditions: 400 °C, 1.5% *n*-butane in air, GHSV = 2400 h^{-1}. (a) VPO_{SC}, (b) VPO_{SCCo}, (c) VPO_{SCacac}. Key: ◆ *n*-butane conversion, ■ maleic anhydride selectivity, □ CO_2 selectivity, × CO selectivity.

It is apparent that, as noted previously,[30] the VPO_{SC} and VPO_{SCacac} catalysts prepared using supercritical CO_2 as an antisolvent do not require any induction time to achieve steady state catalyst performance. In contrast, the standard VPO catalyst prepared from $VOHPO_4{\cdot}0.5H_2O$ require *ca.* 24 h to achieve steady state catalyst performance, a feature that we have commented on previously.[7,10] As expected the addition of 1% Co to crystalline $VOHPO_4{\cdot}0.5H_2O$ results in a catalyst with enhanced catalytic performance (Table 1). By way of contrast, both VPO_{SCCo} and VPO_{SCacac} have much poorer catalytic performances compared with the unmodified VPO_{SC} material. The effect is pronounced and the addition of acetylacetone decreases the specific activity by a factor of *ca.* 2 and a further decrease by a factor of *ca.* 2 is observed on addition of 1 atom % Co. It is therefore apparent that the addition of 1 atom % Co to VPO_{SC} has a significantly different effect when compared to the well studied crystalline VPO catalysts.[8]

Table 1 Catalyst performance data at 400 °C following activation in 1.5% *n*-butane/air for 72 h

Catalyst	Surface area/ $m^2\ g^{-1}$	MA selectivity (%)	Conversion (%)	Intrinsic activity/ 10^5 mol MA $m^{-2}\ h^{-1}$
VPO_{SC}[a]	4	42	15	4.48
VPO_{SCCo}[a]	5	30	4	1.20
VPO_{SCacac}[a]	9	39	9	2.19
VPO[b]	13	39	16	1.20
VPO_{Co}[c]	16	57	36	3.03

[a] GHSV = 2400 h^{-1}. [b] GHSV = 1200 h^{-1}. [c] GHSV = 1000 h^{-1}.

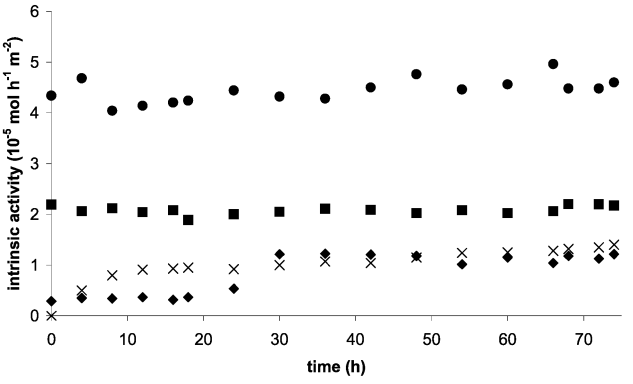

Fig. 2 The intrinsic activity for maleic anhydride (mol $m^2\ h^{-1}$) with time on stream. For VPO catalyst GHSV = 1200 h^{-1}, for all other catalysts GHSV = 2400 h^{-1}. Key: ● VPO_{SC}; ◆ VPO_{SCCo}; ■ VPO_{SCacac}; × VPO.

Catalyst characterisation

The microstructures of VPO and VPO_{Co} crystalline materials have been extensively studied previously.[7,8] In this paper, we concentrate on the characterisation of VPO_{SCCo} and VPO_{SCacac} and compare this with VPO_{SC}. The three materials were found to be amorphous by X-ray powder diffraction both before and after catalyst testing and no discernible Raman spectra could be obtained. Raman and XRD techniques have been used extensively in the study of vanadium phosphate catalysts but in this case they do not provide particularly useful information.[7,10] Hence, we have used three additional techniques to carry out as detailed analysis as possible for the amorphous material, namely transmission electron microscopy, X-ray absorption spectroscopy and ^{31}P spin echo mapping NMR. An analysis of the catalysts prepared using supercritical CO_2 showed that they contained impurities (Fe, 8000 ppm; Cr 2000 ppm, Ni, 800 ppm), which are considered to originate from the apparatus used in their preparation.

Transmission electron microscopy. The VPO_{SC} precursor and catalyst were examined using TEM and representative micrographs of these materials are shown in Fig. 3. The VPO_{SC} precursor [Fig. 3(a)] consists of discrete smooth spherical particles ranging between 75 nm and 2 μm in diameter. These particles show no diffraction contrast (only thickness contrast) and are very prone to electron beam damage. The activated VPO_{SC} catalyst [Fig. 3(b)] is also made up of spherical particles, but these show rougher surfaces and the initial signs of sintering. Many spherical voids, *ca.* 20 nm in diameter, are seen to decorate each particle, arising presumably from the loss of solvent during activation. These give the particles a more dimpled "golf-ball" like appearance. Selected area diffraction pattern analysis of the precursor and activated VPO_{SC} materials

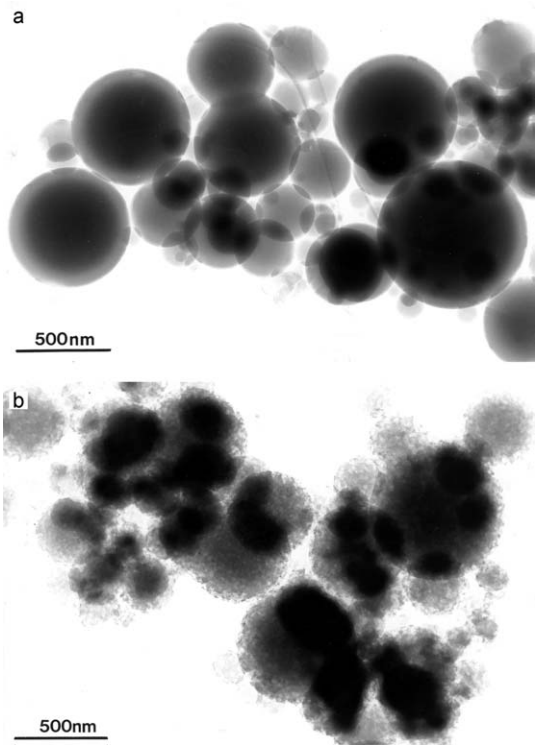

Fig. 3 Bright field transmission electron micrographs of (a) the precursor and (b) the activated VPO_{SC} material.

showed them to be amorphous. This was confirmed by low dose HREM imaging experiments in which neither showed any sign of lattice fringes nor nanocrystalline order.

The precursor and catalyst microstructures of the VPO_{SCCo} and VPO_{SCacac} materials are very similar to each other, but markedly different from that of the VPO_{SC} material in several respects. The precursors [Figs. 4(a) and 5(a)] are again amorphous in character, but now comprise more irregularly shaped

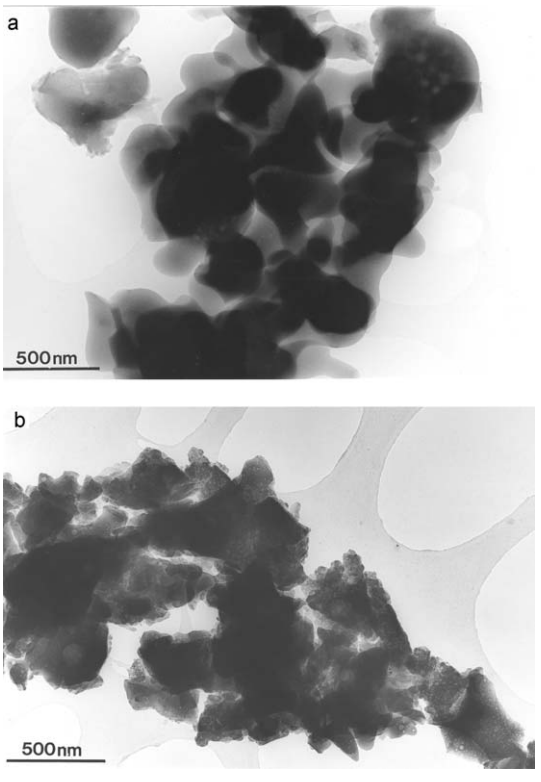

Fig. 4 Bright field transmission electron micrographs of (a) the precursor and (b) the activated VPO_{SCCo} material.

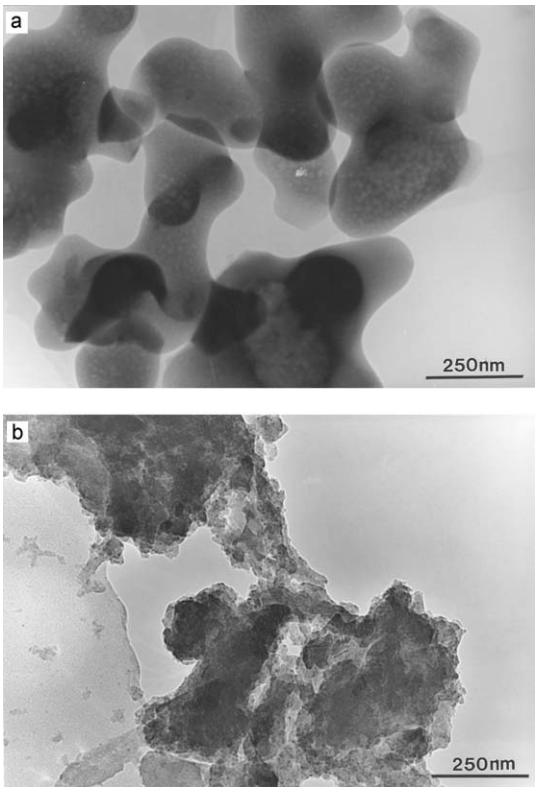

Fig. 5 Bright field transmission electron micrographs of (a) the precursor and (b) the activated VPO_{SCacac} material.

globules that range from 0.2 to 2 μm in size. After activation [Figs. 4(b) and 5(b)], the structure in both cases transforms to a more irregular plate-like structure. Whilst largely disordered in character, HREM and electron diffraction on the VPO_{SCCo} and VPO_{SCacac} activated materials provided some evidence for local crystallinity. However, the poor quality of the crystallographic data and the extreme electron beam sensitivity of the materials made it impossible to make any positive phase identification.

X-ray absorption spectroscopy. X-ray absorption spectroscopy (XAS) in the soft energy range between 100 and 1000 eV is a particularly useful technique for the characterisation of amorphous materials. The vanadium $L_{2,3}$- and the oxygen K-absorption edges of the two precursors, VPO_{SC} and VPO_{SCCo}, are shown in Fig. 6. The vanadium L-edges can be separated into structures corresponding to the $V2p_{3/2} \rightarrow V3d$ (VL_3-edge) and to the $V2p_{1/2} \rightarrow V3d$ (VL_2-edge) transitions. At the oxygen K-edge (at > 528 eV) there are superimposed contributions from the hybridisation of (*i*) O2p states with vanadium and (*ii*) O2p with phosphorus states. By comparison with reference phosphates it can be concluded that the first absorption resonances from 529–535 eV are mainly contributed by O2p/V3d states while the strong features above 534 eV mainly arise from hybridisation of oxygen and phosphorus molecular orbitals. In Fig. 6 it can be seen that all catalysts exhibit three distinct absorption features at 529.3, 530.8 and 532.4 eV, but their relative intensity ratios vary. While for VPO_{SCCo} the first resonance is the most intense, all three resonances are of almost equal intensity for the undoped catalyst VPO_{SC}. This can be interpreted as a significant difference in the V–O bonding configuration as compared to the amorphous sample, which is quite different from the normal crystalline vanadyl pyrophosphate catalysts. The broad resonance around 538 eV, attributed to O/P hybridised electronic states, is most pronounced in the supercritical catalyst VPO_{SC} when compared to the normalised intensity at the vanadium edge.

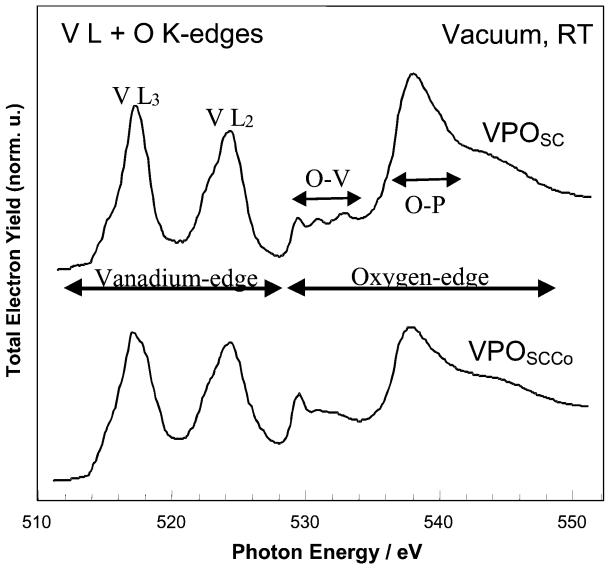

Fig. 6 X-ray absorption spectra at the V $L_{2,3}$- and O K-edges of VPO_{SC} and VPO_{SCCo}. Indicated in the figure is a schematic separation into V L- and O K-absorption edges and areas of main contributions by O-V and O-P electronic orbitals. All spectra were normalised on the intensity maximum at the V L_2-edge.

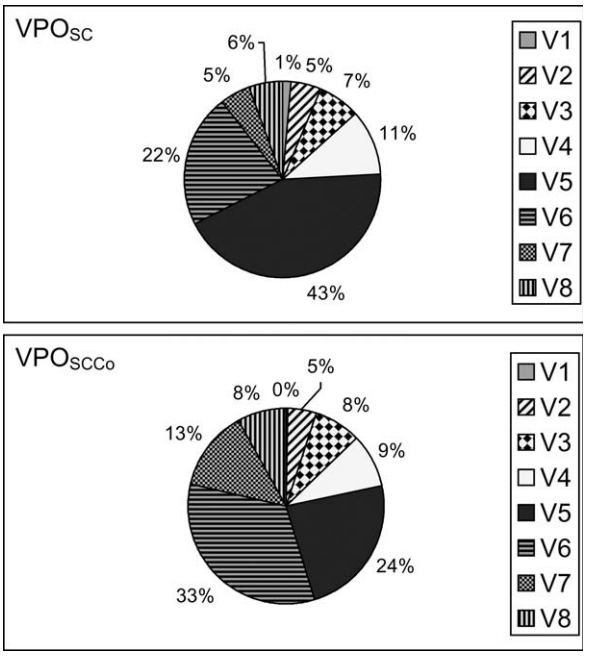

Fig. 8 Spectral weights of resonances V1–V8 for VPO_{SC} and VPO_{SCCo} according to the fit displayed in Fig. 7.

Further analysis was subsequently focussed on the V L_3-NEXAFS shown for VPO_{SC} and VPO_{SCCo} in Fig. 7. Details of the NEXAFS can be interpreted within a framework that relates peak positions to bond lengths.[37] Therefore, analysing the different resonances yields direct information about specific vanadium-oxygen bonds present in the catalyst. At first sight VPO_{SC} and VPO_{SCCo} show a very similar overall spectral function. The resonance positions obtained by an unconstrained least squares fit do not differ by more than 0.2 eV. However, their intensity proportions are different, particularly for the VPO_{SCCo} catalyst, where the resonance V5 around 517.1 eV is not as intense as in VPO_{SC}. This can be seen clearly in the distribution of the spectral weightings normalised in Fig. 8.

It is quite clear from these spectra that the addition of Co dramatically affects the relative distribution of the different vanadium species, which in turn can be expected to have a pronounced effect on their catalytic performances.

^{31}P spin echo NMR spectroscopy. The three activated samples were evaluated by ^{31}P spin echo mapping NMR spectroscopy and the results are shown in Fig. 9. The high number of V^{4+}/V^{5+} dimers is indicated by the strong resonance at 1100 ppm present in all three samples. This is consistent with the amorphous nature of these materials as has been noted previously[30]. However, there are significant differences between the three samples. For both VPO_{SCCo} and VPO_{SCacac} there is a significant increase in the resonance around 2400–3000 ppm, which may be indicative of the presence of some crystalline material such as $(VO)_2P_2O_7$ being present in the sample, which is consistent with the transmission electron microscopy observations. However, both VPO_{SCCo} and VPO_{SCacac} also exhibit a significant resonance at 0 ppm. This can be assigned to phosphate environments and may be indicative of V^{5+} being present. This is consistent with the addition of Co^{2+} oxidising some of the V^{4+} species to V^{5+} in these materials and the increase in the V(V)/V(IV) ration can be observed directly from the relative intensity of the signal at

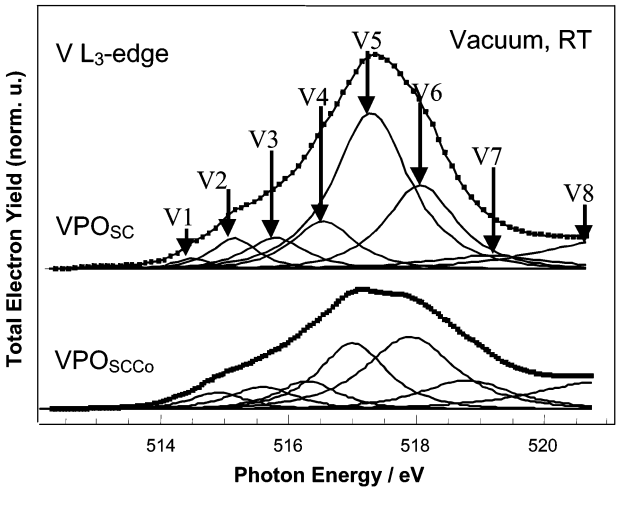

Fig. 7 NEXAFS at the V L_3-edge of VPO_{SC} and VPO_{SCCo}. The fit profiles used are shown and labelled according to their energetic ordering.

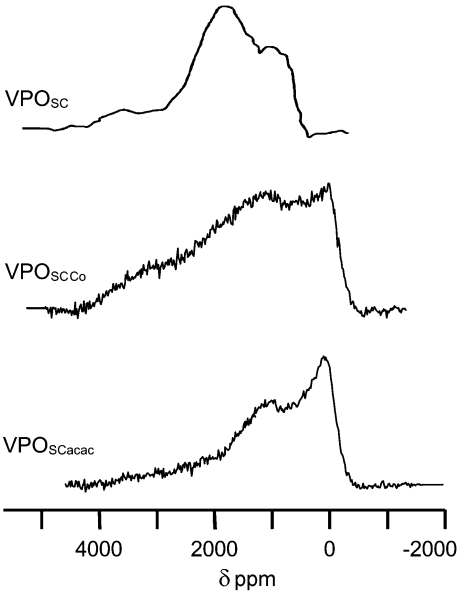

Fig. 9 ^{31}P spin echo NMR spectroscopy of the VPO_{SC}, VPO_{SCCo} and VPO_{SCacac} precursors.

0 ppm. We have noted this effect previously for the vanadium phosphate catalysts[38] where, as the concentration of Co was increased, the amount of V^{5+} phases present (*e.g.*, $VOPO_4{\cdot}2H_2O$) also increased. This would be expected to have a significant effect on the catalytic performance of these materials. It is interesting to consider the origin of the effect of V^{4+} oxidation for the sample prepared using acetylacetone doping alone. We have previously studied the effects of adding large molecules to the preparation of vanadium phosphate catalysts and we have shown that these can act as structural promoters increasing the surface area by being incorporated into the layer structure of the vanadium phosphate.[39] It is possible that this occurs in the present preparation method and the acetylacetone is retained in the amorphous vanadium phosphate following preparation. On subsequent calcination and reaction of butane, the acetylacetone will be oxidised and could lead to a more open structure. This would enable enhanced accessibility of oxygen to vanadium centres in the structure, leading to a potential increase in the oxidation state.

Comments on the effect of Co addition

It is apparent that Co addition to VPO_{SC} results in a material with a lower intrinsic activity (Fig. 2) although the material remains disordered. The transmission electron microscopy study shows that VPO_{SCCo} and VPO_{SCacac} have different morphologies compared with VPO_{SC}, and in particular they do not exhibit the characteristic spherical morphology of the unmodified material. The X-ray absorption spectroscopy study shows that the Co significantly disturbs the different vanadium environments. The ^{31}P spin echo NMR spectra suggest that this is due primarily to oxidation of V^{4+} to V^{5+}. Hence, it is tentatively suggested that Co primarily oxidises the vanadium in the VPO_{SC} material, rather than acting as an electronic promoter.[5,6] It is possible that a different optimal concentration of Co is required for the new amorphous catalysts since catalyst activity is known to be very sensitive to the concentration of Co present.[5,6,8,38] However, from elemental analysis it is apparent that some Fe is also present in the Co-promoted VPO_{SCCo} sample, and the combination of Fe and Co, or their combined concentrations, may be deleterious. However, it is interesting to note that in a previous study of crystalline vanadium phosphate catalysts prepared using aqueous HCl as reducing agent[38] the addition of Co^{2+} leads to oxidation of V^{4+} to V^{5+} with a concomitant reduction in specific activity.

Acknowledgement

We thank the EPSRC for financial support and the staff at BESSY for their continual support during the XAS measurement at the synchrotron in Berlin.

References

1 M. V. Twigg, *Catalyst Handbook*, Wolfe Publishing, Frome, UK, 1999.
2 D. A. King and D. P. Woodruff, *The Chemical Physics of Solid Surfaces*, Elsevier, Amsterdam, 1993, vol. 6.
3 G. J. Hutchings, *Chem. Commun.*, 1999, 301.
4 G. J. Hutchings, *Catal. Lett.*, 2001, **75**, 1.
5 G. J. Hutchings, *Appl. Catal.*, 1991, **72**, 1.
6 G. J. Hutchings and R. Higgins, *J. Catal.*, 1996, **162**, 153.
7 C. J. Kiely, A. Burrows, G. J. Hutchings, K. E. Bere, J. C. Volta, A. Tuel and M. Abon, *Faraday Discuss.*, 1996, **105**, 103.
8 S. Sajip, J. K. Bartley, A. Burrows, C. Rhodes, J. C. Volta, C. J. Kiely and G. J. Hutchings, *Phys. Chem. Chem. Phys.*, 2001, **3**, 2143.
9 M. Otake, *US Pat.* 4337173, 1982.
10 G. J. Hutchings, A. Desmartin Chomel, R. Olier and J. C. Volta, *Nature*, 1994, **368**, 41.
11 V. V. Guliants, J. B. Benziger, S. Sundaresan, N. Yao and I. E. Wachs, *Catal. Lett.*, 1995, **32**, 379.
12 V. V. Guliants, J. B. Benziger, S. Sundaresan, I. E. Wachs, J. M. Jehng and J. E. Roberts, *Catal. Today*, 1996, **28**, 275.
13 V. V. Guliants, S. A. Holmes, J. B. Benziger, P. Heaney, D. Yates and I. E. Wachs, *J. Mol. Catal. A: Chem.*, 2001, **172**, 265.
14 M. R. Thompson, A. C. Hess, J. B. Nicholas, J. C. White, J. Anchell and J. R. Ebner, *Stud. Surf. Sci. Catal.*, 1994, **82**, 167.
15 H. Berndt, K. Buker, A. Martin, A. Bruckner and B. Lucke, *J. Chem. Soc., Faraday Trans.*, 1995, **91**, 725.
16 S. Albonetti, F. Cavani, F. Trifiro, P. Venturoli, G. Calestani, M. L. Granados and J. L. G. Fierro, *J. Catal.*, 1996, **160**, 52.
17 S. Zeyss, G. Wendt, K. H. Hallmeier, R. Szargan and G. Lippold, *J. Chem. Soc., Faraday Trans.*, 1996, **92**, 3273.
18 A. Bruckner, A. Martin, N. Steinfeldt, G. U. Wold and B. Lucke, *J. Chem. Soc., Faraday Trans.*, 1996, **92**, 4257.
19 A. Bruckner, B. Kubias and B. Lucke, *Catal. Today*, 1996, **32**, 215.
20 W. H. Cheng and W. Wang, *Appl. Catal. A*, 1997, **156**, 57.
21 F. Meunier, P. Delporte, B. Heinrich, B. Bouchy, C. Crouzet, C. Phamhuu, C. Panissod, J. L. Leroud, P. L. Mills and M. J. Ledoux, *J. Catal.*, 1997, **169**, 33.
22 K. Ait-Lachgar, A. Tuel, M. Brun, J. M. Herrmann, J. M. Krafft, J. R. Martin, J. C. Volta and M. Abon, *J. Catal.*, 1998, **177**, 224.
23 A. Bruckner, A. Martin, B. Kubias and B. Lucke, *J. Chem. Soc., Faraday Trans.*, 1998, **94**, 2221.
24 A. Martin, G. U. Wolfe, U. Steinike and B. Lucke, *J. Chem. Soc., Faraday Trans.*, 1998, **94**, 2227.
25 P. Delichere, K. E. Bere and M. Abon, *Appl. Catal. A*, 1998, **172**, 295.
26 M. Ruitenbeck, A. J. van Dellen, A. Barbon, E. E. Faassen, D. C. Koningsberger and J. W. Geus, *Catal. Lett.*, 1998, **55**, 133.
27 P. Ruiz, P. Bastians, L. Caussin, R. Reuse, L. Daza, D. Acosta and B. Delmon, *Catal. Today*, 1993, **16**, 99.
28 H. Morishige, J. Tamaki, N. Msura and N. Yamazoe, *Chem. Lett.*, 1990, 1513.
29 S. Sajip, C. Rhodes, J. K. Bartley, A. Burrows, C. J. Kiely and G. J. Hutchings, in *Catalytic Activation and Functionalisation of Light Alkanes*, ed. E. G. Derouane, Kluwer, The Netherlands, 1998, p. 429.
30 G. J. Hutchings, J. K. Bartley, J. M. Webster, J. A. Lopez-Sanchez, D. J. Gilbert, C. J. Kiely, A. F. Carley, S. M. Howdle, S. Sajip, S. Caldarelli, C. Rhodes, J. C. Volta and M. Poliakoff, *J. Catal.*, 2001, **197**, 232.
31 J. Li, M. E. Lashier, G. L. Schrader and B. C. Gerstein, *Appl. Catal.*, 1998, **38**, 83.
32 M. T. Sananes, A. Tuel and J. C. Volta, *J. Catal.*, 1994, **145**, 251.
33 M. Hävecker, A. Knop-Gericke, T. Schedel-Neidrig and R. Schlögl, *Angew. Chem.*, 1998, **110**, 2049*Angew. Chem., Int. Ed.*, 1998, 37, 206.
34 A. Knop-Gericke, M. Hävecker, T. Schedel-Neidrig and R. Schlögl, *Top. Catal.*, 2001, **15**, 27.
35 K. J. S. Sawhney, F. Senf, M. Scheer, F. Schäfer, J. Bahrdt, A. Gaupp and W. Gudat, *Nucl. Instrum. Methods Phys. Res., Sect. A*, 1997, **390**, 395.
36 M. Hävecker, A. Knop-Gericke, R. W. Mayer, H. Bluhm and R. Schlögl, in preparation.
37 G. Comelli, J. Stöhr, C. J. Robinson and W. Jark, *Phys. Rev. B*, 1998, **38**, 7511.
38 G. J. Hutchings, I. J. Ellison, M. T. Sananes and J. C. Volta, *Catal. Lett.*, 1996, **38**, 231.
39 J. Cabello Sanchez, J. A. Lopez-Sanchez, R. P. K. Wells, C. Rhodes and G. J. Hutchings, *New. J. Chem.*, 2001, **25**, 1528.